

## Magnesium Alloys for Hydrogen Storage Processed by ECAP Followed by Low Temperature Rolling

W.B. Silva<sup>a\*</sup> , D.R. Leiva<sup>b</sup>, R. Floriano<sup>c</sup>, L.E.R. Vega<sup>a</sup>, V.B. Oliveira<sup>d</sup> , J. Gallego<sup>e</sup> ,  
S.J.A. Figueroa<sup>f</sup>, E.X. Miqueles<sup>f</sup>, E.P. Silva<sup>g</sup>, T.T. Ishikawa<sup>b</sup>, W.J. Botta<sup>b</sup>

<sup>a</sup>Universidade Federal de São Carlos, Programa de Pós-Graduação em Ciência e Engenharia de Materiais, Rod. Washington Luis, km 235, CEP 13565-905, São Carlos, SP, Brasil.

<sup>b</sup>Universidade Federal de São Carlos, Departamento de Engenharia de Materiais, Rod. Washington Luis, km 235, CEP 13565-905, São Carlos, SP, Brasil.

<sup>c</sup>Universidade Estadual de Campinas (UNICAMP), Faculdade de Ciências Aplicadas (FCA), Pedro Zaccaria, 1300, 13484-350, Limeira, SP, Brasil.

<sup>d</sup>Universidade do Estado do Rio de Janeiro, Instituto Politécnico, Departamento de Materiais, Nova Friburgo, 28.625-570, Rio de Janeiro, RJ, Brasil.

<sup>e</sup>Universidade Estadual Paulista (UNESP), Departamento de Engenharia Mecânica, Avenida Brasil, 56, 15385-000 Ilha Solteira, SP, Brasil.

<sup>f</sup>Laboratório Nacional de Luz Síncrotron (LNLS), Centro Nacional de Pesquisa em Energia e Materiais (CNPEM), 13083-970, Campinas, SP, Brasil.

<sup>g</sup>Universidade Federal do Vale do Jequitinhonha e Mucuri, Instituto de Engenharia, Ciência e Tecnologia (IECT), Departamento de Engenharia de Materiais, Janaína, MG, Brasil.

Received: May 04, 2021; Revised: January 21, 2022; Accepted: February 03, 2022

The hydrogen storage properties of pure magnesium and magnesium ZK60 alloy containing 2.5 wt% of *mischmetal* (Mm) processed by Cold Rolling (CR) and Low Temperature Rolling (LTR) were investigated. Before CR and LTR processing, Equal Channel Angular Pressing (ECAP) was employed in the alloys as an initial processing step to refine their microstructures. Microstructure findings showed that the ECAP+LTR route is more effective than the others to generate grain refinement - a desirable aspect in hydrogen storage materials. SEM and TEM results in combination with XPS analysis revealed that the ZK60 + 2.5 wt. % Mm alloy after being processed by ECAP + LTR had more refined grains (with sizes < 1 μm) and exhibited superior resistance to the formation of oxides and/or hydroxides when compared with the pure magnesium alloy. The refined microstructures of the ECAP+LTR samples combined with the presence of highly oriented grains along to the (002) plane and large amount of defects – which are features associated to the LTR route - such as cracks and voids, resulted in a fast activation kinetics than for the samples processed by ECAP + CR route.

**Keywords:** Mg-Alloys, Low-Temperature rolling, ECAP, Hydrogen storage, Metal hydrides.

### 1. Introduction

Due to the problems produced by the intense use of the fossil fuels, hydrogen is considered as an alternative energy carrier in the near future. The challenge of spreading the hydrogen technology worldwide is clearly related to the need to develop feasible and effective storage methods<sup>1,2</sup>. Several studies addressing hydrogen storage conducted by various research groups have demonstrated that hydrogen storage in metal hydrides in the solid-state form is an excellent option for hydrogen storage offering high volumetric hydrogen storage capacity, safety and reliability, as well as high purity of the supplied H<sub>2</sub> in comparison to the hydrogen storage in a tank of compressed gas or liquid hydrogen<sup>1-4</sup>.

Magnesium (Mg) and its alloys have been proven to be promising candidates for hydrogen storage applications due

to their excellent gravimetric capacity, availability and low price<sup>5-10</sup>. Furthermore, Mg-based hydrides present interesting functional properties, such as reversibility and long-term cyclability<sup>6</sup>. However, the unfavorable sorption properties, high thermodynamic stability and slow H<sub>2</sub> absorption/desorption kinetics of Mg-based materials, also including the high reactivity of those compounds with air and humidity from the environment, their application has been limited<sup>11</sup>.

Nevertheless, it is widely known that processing by high-energy ball milling (HEBM) in combination with the addition of selected additives/catalyst in the nanostructuring of Mg-based alloys promoted a beneficial effect on its hydrogen storage characteristics, enabling even at lower temperatures faster kinetics. But, two important issues should be taken into account when we select the HEBM as the main processing route to the production nanostructured Mg-based materials with desirable properties for hydrogen

\*e-mail: [wagnerbatista@ppgcm.ufscar.br](mailto:wagnerbatista@ppgcm.ufscar.br)

storage: a) the HEBM requires longer processing times associated with high energy consumption that increase the total cost of processing; b) the powders obtained by HEBM display high specific surface area, and therefore, they are substantially vulnerable to air contaminants as oxygen or humidity, demanding, a complex handling that should be done under inert atmosphere<sup>12</sup>. In this context, the use of Severe Plastic Deformation (SPD) techniques such as Equal Channel Angular Pressing (ECAP), Cold Rolling (CR) and Friction Stir Processing (FSP) as alternative processing routes for Mg-based materials aiming desirable hydrogen storage properties has been demonstrated to be a successful approach to address these issues<sup>13-19</sup>.

The simplicity, economy and proximity to industrial practice, since they are generally performed in the air, with processing normally in a short period of time (minutes or seconds), are the main gains of using SPD techniques in contrast with HEBM. Beyond that, SPD techniques, in particular ECAP and CR, are also effective for changing the hydrogen storage characteristics of the material by providing nano-sized grains and also the inclusion of high density of defects and cracks which are favorable aspects for hydrogen storage in materials<sup>12-13, 20-22</sup>.

In the study of Lima et al.<sup>23</sup>, commercial Mg ingots were processed by using the combination of ECAP followed by CR techniques aiming better hydrogen storage properties. They observed fast hydrogen kinetics and high absorption capacity (5.7 wt% of H<sub>2</sub>) when compared with samples only processed by ECAP (1.5 wt% of H<sub>2</sub>). They attributed these good hydrogen storage properties to the favorable orientation along to (002) direction related to the  $\alpha$ -Mg grains associated with the high density of defects resulted by CR, which can operate as preferential nucleation centers for hydride formation.

Soyama et al.<sup>13</sup> investigated the effects of CR processing in commercial magnesium ZK60 alloy altered with the addition of 2.5 wt % of *mischmetal* (Mm). The alloys were initially processed by ECAP or melt spinning (MS), both followed by extensive cold rolling at room temperature. The results indicated that the additional processing by CR in the ECAPed and MSed samples caused further grain refinement and breakage of intermetallic particles, as well as favoring crystallographic texture in the (002) direction. The intermetallics coming from the addition of *mischmetal* were very small and distributed within and along grain boundaries. All these factors provided a notable progress in the absorption kinetics and in the hydrogen storage capacity of the samples performed only by MS and ECAP. The authors also highlighted the catalytic effect of the fine secondary phases dispersed in the alloy due to the cold rolling processing, which could act as nucleation sites for the hydride phase formation.

In another study, Floriano et al.<sup>24</sup> evaluated the hydrogen storage properties of the commercial AZ91-Mg alloys after processing by CR at room temperature and CR under low temperature (also called: Low temperature rolling – LTR), in this case, the liquid nitrogen temperature. The innovator process applied in this study was established on the rolling of the AZ91 samples after the submersion in the liquid nitrogen a certain time, which guaranteed the sample a

greater pre-rolling fragility. This excessive fragility resulted in an important spreading of cracks and elevated surface area/volume ratio of the AZ91. The samples processed by LTR showed higher hydrogen storage capacity and faster hydrogen kinetics (including activation) when compared with those samples solely processed by CR. These main findings were attributed to the existence of a finer grain structure, the larger number of cracks and the cold-welded overlapping surface layers formed in the LTR sample in relation to the CR sample, resulting in larger surface area. Based on the results presented in this study, the LTR processing route demonstrated to be a potential processing route for hydrogen storage materials.

More recently, Silva et al.<sup>18</sup> studied the hydrogen storage properties on commercial ZK60-Mg alloy processed by FSP followed by manual filing. The results showed that filings taken out from the stir zone (SZ) presented much faster kinetics of hydrogen absorption than those from the as-cast (AC) condition. This finding was attributed to the major presence of nanometric second-phase intermetallic particles (Mg<sub>7</sub>Zn<sub>3</sub>) distribution in the SZ. However, the catalytic effect of Mg<sub>7</sub>Zn<sub>3</sub> intermetallic on hydrogen storage properties could not be evaluated in detail since they dissolve in a temperature below (~ 343,4 °C) to the temperature employed for measuring the absorption/desorption kinetics (350 °C)<sup>25</sup>.

Silva et al.<sup>24</sup> also showed that the Mm added in the ZK60-Mg alloy led to the precipitation of the MgZn<sub>2</sub>Ce phase which presented higher dissolution temperature (up to 460 °C), enabling the study of its catalytic effect on the hydrogen storage properties of the ZK60-Mg alloys processed by cold rolling followed by manual filing. It was observed that the addition of small fraction of Mm in Mg alloys not only decreases their rates of decrepitation and increases their cyclic stability but also could lead to an increase in the hydride equilibrium pressure, promoting faster absorption/desorption kinetics at 350 °C. However, the addition of Mm in Mg alloys can also contribute to the reduction in the hydrogen storage capacity of alloys<sup>26-27</sup>. At small concentrations (<10 wt.%), Mm<sup>28</sup> or rare earth elements such as La, Ce, Y, among others can act as preferential nucleation sites for the hydride formation in Mg-based alloys<sup>29-30</sup>.

In the present study, we evaluated the hydrogen storage properties of two different materials: i) pure Mg; and ii) the commercial ZK60 magnesium alloy modified by the addition of 2.5 wt% of Mm; both materials were processed by CR and LTR. Before the processing by CR and LTR, the Mg-based samples were initially submitted to ECAP to obtain an initial microstructure containing a desirable orientation and a reasonable number of defects as internal cracks/voids and grain boundary interfaces that can be considered favorable aspects to improve the hydrogen storage properties as already mentioned in our previous studies. In summary, three main aspects were addressed in this present study: i) the comparison between the H<sub>2</sub> storage properties of commercial ZK60 Mg alloy modified by addition of 2.5 wt% of Mm and the pure Mg; ii) the investigation of the effects of LTR and CR processing on Mg- based samples; iii) the potential of ECAP as a primary processing route to prepare a microstructure with desirable aspects for hydrogen storage studies.

## 2. Experimental

The experiments were carried out using pure Mg and the ZK60-Mg alloy modified with 2.5 wt% Mm (55% Ce, 26% La, 15% Nd, and 4% Pr) in the as-cast condition. More details about the processing of the ZK60 magnesium alloy modified with 2.5 wt% Mm can be found in the reference<sup>31</sup>. ECAP was performed using the B<sub>2</sub> route as indicated in reference<sup>32</sup>. Four consecutive passes at 300 °C and 9 mm/min of run speed were employed. A graphite-based lubricant was used to reduce friction between the surfaces of the samples and the matrix. All processing by ECAP was performed employing a solid die with an internal channel angle of  $\Phi=110^\circ$  and an angle at the outer arc of curvature of the two parts of the channel of  $\psi=20^\circ$ . ECAPed samples for subsequent CR and LTR processing were cut transversely into 2 mm-thick samples. CR and LTR were carried out in a duo-reversible FENN rolling mill under air atmosphere. To reach the temperature of liquid nitrogen (LN<sub>2</sub>), the LTR samples were subjected to LN<sub>2</sub> immersion cooling for 3 min, just before the first rolling pass and then after every five rolling passes. After LN<sub>2</sub> immersion, the samples were placed between two stainless steel plates (at room temperature) to avoid contamination and were then rolled again until they became foil-shaped with an average thickness of 0.17 mm. A similar procedure was done for the CR samples but excluding the LN<sub>2</sub> bath.

The structural characterization of the processed samples was carried out by X-ray diffraction (XRD) using a Siemens D5005 X-Ray diffractometer radiation operating at 40 KV and 40 mA with Cu K $\alpha$  radiation ( $\lambda = 0.15406$  nm). The XRD patterns were obtained in the longitudinal direction of the rolling surfaces of samples using a 2theta interval from 25° to 75° with a step size of 0.032°.

Microstructural characterization was performed by using scanning electron (SEM) and optical (OM) microscopy. SEM images were obtained in a FEG-XL30 Phillips microscope. OM images were carried out in an Olympus BX41-LED microscope. In order to investigate finer microstructural details, a Philips CM-120 transmission electron microscope (TEM) was also used. All images were recorded digitally and further analyzed by using Image J software.

X-ray photoelectron spectroscopy (XPS) was employed to carry out the surface analyses. It was measured at the National Nanotechnology Laboratory (LNNano) at the National Center for Research in Energy and Materials (CNPEM), in the city of Campinas, SP, Brazil. Measurements were performed in the conventional mode on a Thermo Scientific model K-Alpha. For data treatment purposes, the energy was corrected based on the peak of C 1s (Adventitious Carbon = 284.8 eV) and measured with energy of 1486.6eV through Al k-alpha anode with a spot size close to 400 micrometers. The samples were manipulated with gloves reduced to pieces with dimensions of 5 mm x 5mm with a stainless steel cutter and deposited onto a carbon tape at the bottom, with the samples always cover the carbon tape. Measurements were repeated 5 times in 3 different positions on the same sample in order to have a representative measurement of the surface. In all cases, there were no differences between the measurements in similar samples and finally an average was determined. Spectral data was treated using the CasaXPS software (version 2.3.19). Quantification of the original XPS spectra was performed by

adjusting the components under the peaks and calculating their area for revealing details about the shape and composition of internal structures of the material.

X-ray Microtomography was used to determine the fraction of defects. The technique was employed using a IMX beamline (<https://www.lnls.cnpem.br/facilities/imx-en/>) at the Brazilian Synchrotron Light Laboratory (LNL), after prior tests in a LNNano MicroCT facility that cannot give us the ultimate resolution. In the IMX beamline, three-dimensional reconstruction volumes were generated by a monochromatic parallel X-ray beam hitting the sample. The reconstruction process was carried out using the filtered-back projection algorithm through the analytical strategy described in reference<sup>33</sup>, suitable for fast processing of large measured 3D data. The samples were manipulated with gloves reduced to pieces with dimensions of 2 mm x 5mm with a stainless steel cutter and glued onto a pin with some wax. Reconstructed volumes were taken far away from the edges of the material inside the bulk.

The hydrogen storage behavior in the Mg-based samples was investigated by measuring the activation and absorption/desorption kinetic measurements using a homemade Sievert's type volumetric apparatus. The foil-shaped samples with 100 mg mass were cut into pieces with dimensions of 5 x 5 x 0.17 mm and placed in a stainless steel cell with an internal volume of 6.4 cm<sup>3</sup>. Each sample was heated under vacuum until the stabilization of the temperature at 350 °C for the H-absorption/desorption kinetic measurements. Hydrogen pressures of 20 bar and 1 bar were used for absorption and desorption, respectively. Experimental contents (in percentage) of the absorbed/desorbed hydrogen are presented as a fraction of the 7.6 and 6.5 wt% which are the theoretical storage capacities for pure Mg and the ZK60-Mg alloy with 2.5 wt% of Mm, respectively.

## 3. Results and Discussion

Figure 1a-b show, respectively, the optical micrographs for pure Mg and ZK60-Mg alloy modified by the addition of 2.5 wt% of Mm both in the as-cast state. The pure magnesium sample shows the presence of  $\alpha$ -Mg grains larger than 500  $\mu$ m. It is also observed that deformation twins appear distributed within the  $\alpha$ -Mg grains, as a result of the metallographic sample preparation<sup>34</sup>. Meanwhile, the ZK60+2.5Mm alloy is constituted by  $\alpha$ -Mg globular grains with an average size of 200  $\mu$ m and these grains are derived from the mechanical beat<sup>35,36</sup> applied during the arc-melting process resulting in a uniform distribution of grains in the solidification structure of the alloy. A dendritic network of the intermetallic MgZn and/or MgZnRE phases was also observed inside the  $\alpha$ -Mg grains which is typical of the as-cast solidification microstructure<sup>35,36</sup>.

Figure 2 presents the XRD patterns of the pure Mg (Figure 2a) and ZK60+2.5Mm (Figure 2b) alloy after performing ECAP+CR and ECAP+LTR. The XRD patterns of these samples in the as-cast state were also included for comparison. The XRD patterns were normalized according to the relative intensity of the highest intensity peak. For samples in the as-cast state, we assigned 100% to peak 101, and the intensities of the other peaks (002 and 100)

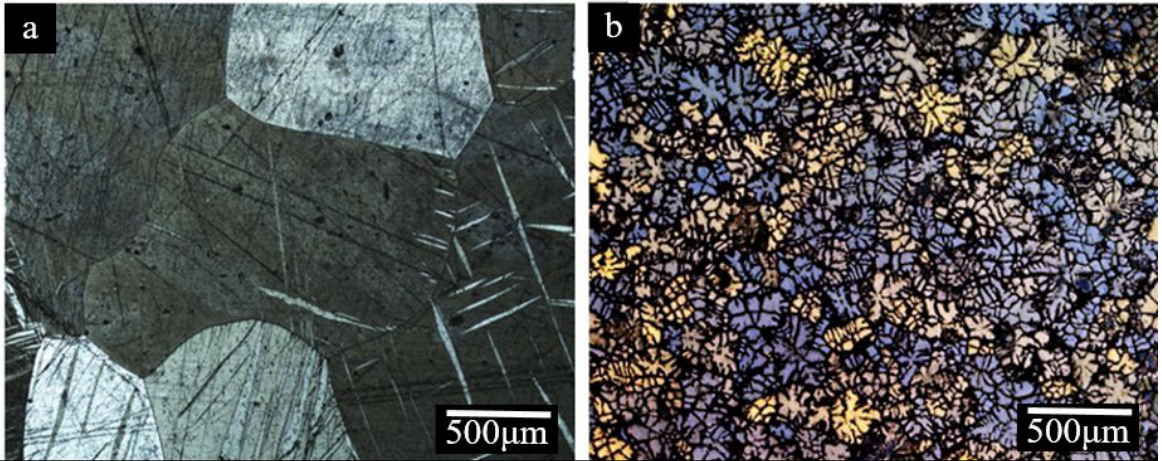


**Figure 1.** Optical microscopy images obtained with polarized light for (a) pure Mg and (b) ZK60 + 2.5Mm alloy in the as-cast state.

**Table 1.** Summary of relative intensity of the planes related to the  $\alpha$ -Mg peaks.

Material/ Processing route		Relative intensity (%) of the preferred planes		
		(100)	(002)	(101)
Pure Mg	As-cast	20	86	100
	ECAP+CR	1	100	4
	ECAP+LTR	1	100	3
ZK60+2.5Mm	As-cast	14	18	100
	ECAP+CR	5	100	27
	ECAP+LTR	6	100	39

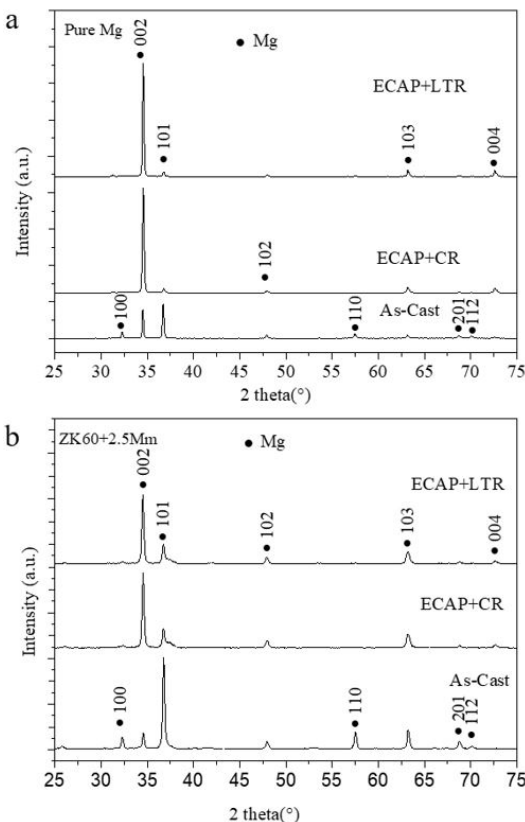


**Figure 2.** XRD patterns of pure Mg (a) and ZK60+2.5Mm (b) alloy in the AC, ECAP+CR and ECAP+LTR states.

are related to this peak; for the other samples, we assigned 100% to peak 002.

As can be seen in these XRD patterns, the samples showed the presence of the majority  $\alpha$ -Mg phase with hexagonal structure. However, the presence of intermetallic phases such as MgZn and/or MgZnRE (as observed in Figure 1) was not detected in the ZK60-Mg alloy modified by the addition of Mm (Figure 2b) probably due to its lower amount being below to the detection limit of XRD technique. It is worth noting that there is a high preferential orientation in association with the (002) type texture for the samples processed by ECAP+CR and ECAP+LTR.

Table 1 displays the summary of relative intensities for the planes (100), (002) and (101) belonging to the  $\alpha$ -Mg phase, showing which are the preferably planes oriented after processing. As can be observed for the pure Mg sample, the intensity of (002) basal plane increases from 86% in the as-cast condition to 100% after processing by ECAP+CR and ECAP+LTR. In a similar way for the ZK60+2.5Mm alloy, the intensity of (002) basal plane increases from 18% in the as-cast condition to 100% after processing by ECAP+CR and ECAP+LTR, respectively. The preferred orientation of the (002) basal plane is stronger in pure Mg sample than in the ZK60 + 2.5Mm alloy samples after processing. It is well known that slip is preferred in more compact planes, such as the (002) basal planes in magnesium-based materials<sup>37</sup>. The presence of the second phases such as the intermetallics in the ZK60+2.5Mm alloy influenced the stiffness for the (002) basal plane sliding, thus favoring sliding of other planes, as occurred for plane (101). In addition, increased intensity of the (002) peak in  $\alpha$ -Mg-based materials processed by CR

and LTR has also been reported in previous studies and this feature seems to improve their hydrogen absorption/desorption properties<sup>23,38-43</sup>.

Figure 3 (a-c) shows SEM images obtained using the secondary electrons (SE) signal for the pure Mg processed by ECAP, ECAP+CR and ECAP+LTR routes. These images reveal that the as-cast  $\alpha$ -Mg grains were reduced from sizes larger than 500  $\mu\text{m}$  (Figure 1a) to approximately 45  $\mu\text{m}$  (Figure 3a) after ECAP. However, an ultra-grain refinement followed by a homogeneous distribution of the  $\alpha$ -Mg grains can also be observed in the samples after processing by ECAP+CR and ECAP+LTR. Such type of microstructure is associated with the dynamic recrystallization phenomena that occur completely during the four ECAP passes<sup>12</sup>. In addition, deformation twins were developed and are likely to contribute to the  $\alpha$ -Mg grain refinement in this material<sup>44</sup>.

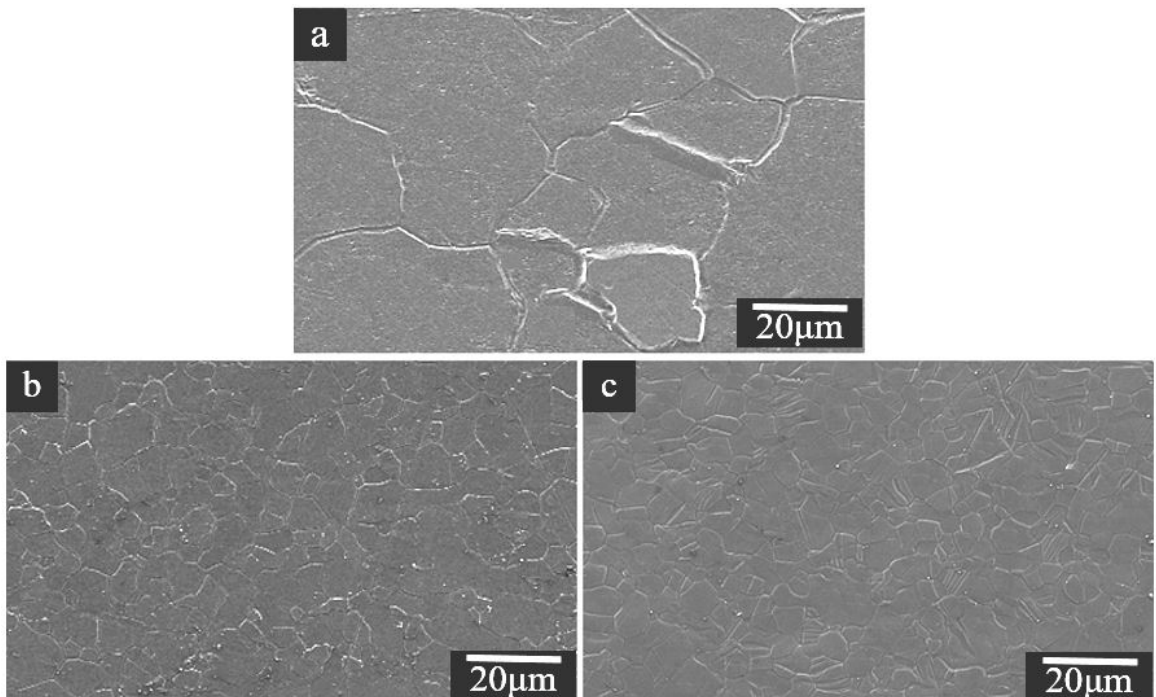
We could also see that the processing by ECAP+CR can refine grains more effectively (Figure 3b) since a heterogeneous structure with  $\alpha$ -Mg grains with sizes of around 7  $\mu\text{m}$  (Figure 3b) was observed in SEM images. But, the combination of ECAP followed by LTR resulted in the most efficient processing route combination among all routes leading to the extremely refinement of  $\alpha$ -Mg grains to around 4  $\mu\text{m}$  (Figure 3c). As the processing was carried out at room temperature and LTR, the occurrence of recrystallization should not occur. However, the grains did not elongate along the rolling direction. Jorge et al.<sup>40</sup> who also worked with magnesium processed by ECAP+CR observed a grain structure similar to that observed in this work.

In the study of Edalati et al.<sup>45</sup>, the authors identified that the grain refining in pure Mg after processing by HPT at cryogenic temperatures could not be carried out much more

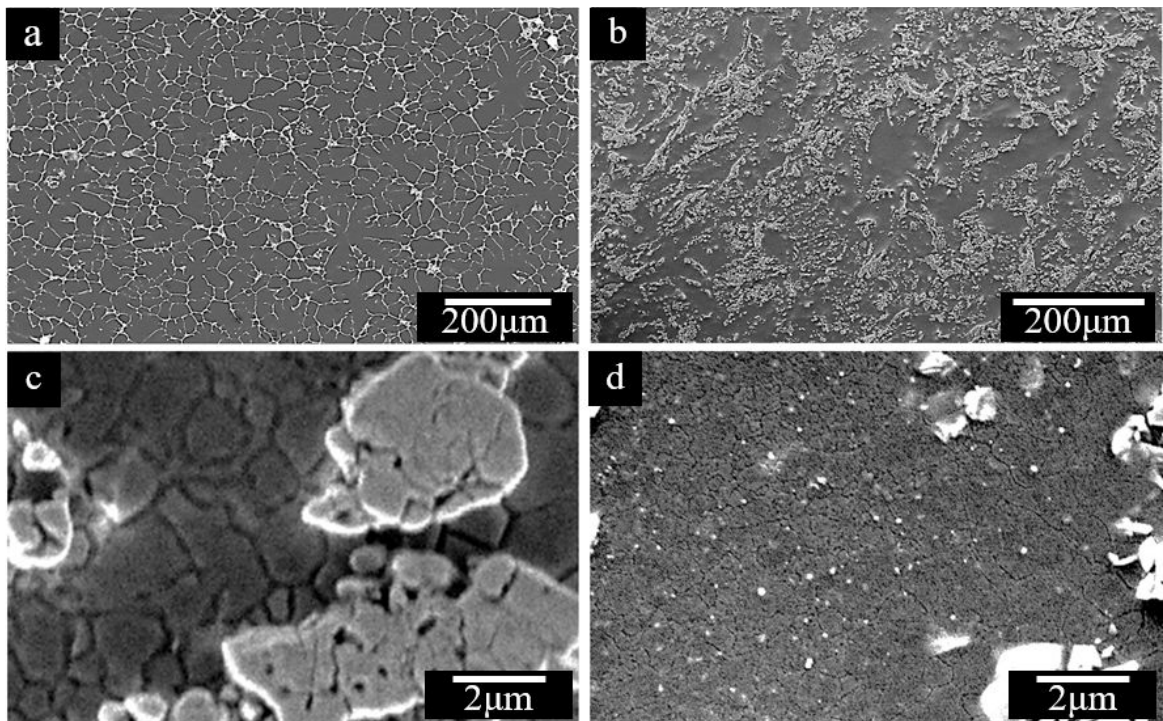
efficiently than at room temperature. The sample processed at 300 K had an average grain size of 1  $\mu\text{m}$  while the one processed at 100 K had an average size of 2.7  $\mu\text{m}$ .

Figure 4 displays SEM images of the ZK60+2.5Mm alloy in the as-cast state and after processing by ECAP+CR and ECAP+LTR. It can be observed that the as-cast ZK60+2.5Mm alloy (Figure 4a) exhibits a dendritic network of intermetallic phase that grows from interior of the  $\alpha$ -Mg phases towards the grains boundaries as already observed in Figure 1.

As can be noticed in the SEM images (Figure 4b-d), a remarkable grain refinement accompanied by a dispersion of intermetallic phases in the ZK60+2.5Mm samples were achieved after processing by ECAP+LTR and ECAP+CR. In these SEM images, it is possible to observe the presence of a structure composed by  $\alpha$ -Mg grains with sizes ranging from 0.3 to 2  $\mu\text{m}$ . Moreover, after CR and LTR processing, the dendritic network of intermetallics was broken into small particles (Figure 4b). It is likely that the low ductility together with the cryogenic condition facilitate the breaking of such intermetallic particles, promoting new interfaces that could be beneficial for the hydrogen storage properties of this alloy<sup>19,46</sup>. In the alloy performed by ECAP+CR (Figure 4c) condition, a structure of  $\alpha$ -Mg grains was also observed with sizes from 0.5 to 2  $\mu\text{m}$ , which was larger than the samples processed by ECAP+LTR. This feature can be understood by considering that the LTR processing may have promoted a significant increase in dislocation density accompanied by lower stacking fault energy due to dynamic recovery suppression at low temperature<sup>25,47</sup>, thus facilitating deformation<sup>48</sup> and, consequently, more intense grain refinement.



**Figure 3.** SEM images obtained using the Secondary Electron (SE) signal for pure Mg after processing by: (a) ECAP; (b) ECAP+CR; (c) ECAP+LTR.



**Figure 4.** SEM images of ZK60+2.5Mm alloy after (a) as-cast and (b) ECAP+LTR in the BSE mode; (c) ECAP+CR and (d) ECAP+LTR in the SE mode.

Figure 5 shows bright field (BF) and dark field (DF) TEM images with Selected Area Electron Diffraction pattern (SAED) for the pure Mg and ZK60+2.5Mm alloy after ECAP+LTR. BF images reveal the extension of the microstructure deformation in pure Mg (Figure 5a) and ZK60+2.5Mm alloy (Figure 5c). These TEM images reveal that the deformation level is higher within  $\alpha$ -Mg grains for the pure magnesium than for the ZK60+2.5Mm alloy, which corresponds to the presence of a more refined and deformed (or less recrystallized) microstructure in the pure Mg sample. Strong diffraction spots observed in the SAED image (Figure 5d) also indicate the development of less deformed  $\alpha$ -Mg grains, most likely due to the more intense recrystallization and random recrystallization texture in the ZK60+2.5Mm alloy than in pure Mg.

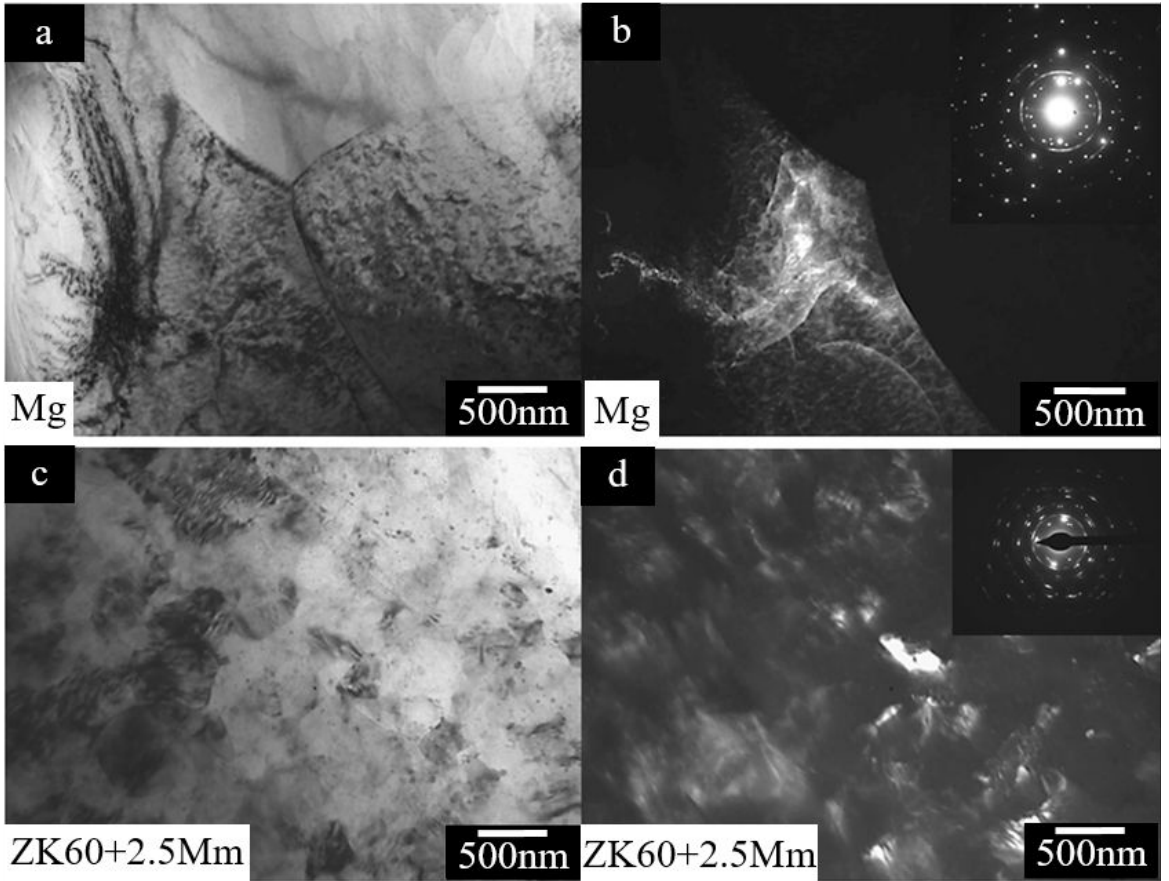
As all processing routes were performed under air, XPS analysis was conducted in order to evaluate the level of surface oxidation especially in the samples after processing by ECAP+LTR. Figure 6a-b show, respectively, the XPS spectra of the Mg-2p peak for the pure Mg and ZK60+2.5Mm alloy after processing by ECAP+LTR. In these XPS spectra, the deconvolution of peaks was also included.

Table 2 summarizes the information extracted from XPS analysis. Firstly, it can be observed that Mg was detected in the elemental form (metallic Mg) and also in the form of oxides and hydroxides in both materials. Metallic Mg corresponds to the largest peak which refers to 24.2% and 28.0% in area for Mg pure and ZK60+2.5Mm alloy, respectively. However, magnesium oxide/hydroxide content is slightly higher in pure Mg than in the ZK60+2.5Mm alloy (75.8% vs 72.0%).

The presence of MgO/Mg(OH)<sub>2</sub> can be understood as a consequence of association of water condensation on the exposed surfaces of the samples (after LN<sub>2</sub> immersion cooling) in interaction with oxygen from the atmospheric air. With reference to the ZK60+2.5Mm alloy, the low amount of magnesium oxides/hydroxides demonstrates that probably its air resistance to contamination was slightly improved by the addition of Zn (from the alloy) and 2.5 wt.% of Mn.<sup>49</sup> This suggests that the behavior of the hydrogen storage properties of these Mg-based materials, under the same processing condition, could be very different from each other since the presence of MgO/Mg(OH)<sub>2</sub> species may contribute to their hydrogen storage degradation<sup>24,50</sup>.

As the measurements were repeated 5 times at 3 different positions in the same sample to have a representative surface measurement and in all cases, there were no differences between measurements in the same sample, the results are strongly representative of the actual condition of the surfaces of the analyzed samples.

Synchrotron-radiation X-ray microtomography was used to assess the volume of cracks in the pure Mg and in the ZK60+2.5Mm samples after processing by ECAP+CR and ECAP+LTR. Table 3 summarizes the cracks volume fraction ( $V_c$ ), the reconstructed sample volume ( $V_r$ ) and the relationship between these parameters ( $V_c/V_r$ ), as determined by microtomography reconstructions. Firstly, as can be observed, the ZK60+2.5Mm alloy showed a higher  $V_c/V_r$  ratio in comparison with the pure Mg sample, independently of the processing route employed. The high  $V_c/V_r$  ratio in the alloy is related to the higher occurrence of superficial (cracks) and internal (voids) defects in this sample when



**Figure 5.** TEM images in BF (Figure 5a-c) and DF (Figure 5b-d) mode of pure Mg and ZK60+2.5Mm alloy after ECAP+LTR processing route.

**Table 2.** Curve fitting parameters from XPS spectra of the Mg-2p peak.

Samples after ECAP+LTR	Type of species	Peak energy (eV)	Area (%)
ZK60+2.5Mm	metallic Mg	49.9	28.0
	MgO/Mg(OH) <sub>2</sub>	50.8	72.0
Pure Mg	metallic Mg	49.9	24.2
	MgO/Mg(OH) <sub>2</sub>	50.8	75.8

**Table 3.** Crack volume fraction ( $V_c$ ) and reconstructed sample volume ( $V_r$ ) as determined by microtomography reconstructions for pure Mg and ZK60 + 2.5Mm alloy after ECAP + CR and ECAP + LTR processing routes.

Sample	$V_c$ (mm <sup>3</sup> )	$V_r$ (mm <sup>3</sup> )	$V_c/V_r$
Mg/ECAP+CR	$1.15 \times 10^{-4}$	2.85	$4.03 \times 10^{-5}$
Mg/ECAP+LTR	$2.00 \times 10^{-4}$	2.10	$9.04 \times 10^{-5}$
ZK60+2.5Mm/ECAP+CR	$3.24 \times 10^{-4}$	1.66	$1.95 \times 10^{-4}$
ZK60+2.5Mm/ECAP+LTR	$5.86 \times 10^{-4}$	1.40	$4.19 \times 10^{-4}$

compared to the pure Mg. Regarding to processing routes comparison, it is evident that the combination of ECAP+LTR is more effective than ECAP+CR in generates a larger amount of defects in the samples. Thus, the highest value of  $V_c/V_r$  ratio was observed for the ZK60+2.5Mm alloy performed by ECAP+LTR.

Experimental contents of the absorbed/desorbed hydrogen storage capacity from 0 to 1 are presented as a fraction of the 7.6 and 6.5 wt.% which are the theoretical storage capacities

for pure Mg and the ZK60-Mg alloy with 2.5 wt.% of Mm, respectively.

Figure 7 (a-d) displays the activation and first hydrogen desorption kinetic curves at 350 °C under 20 bar of hydrogen pressure for pure Mg and for ZK60+2.5Mm alloy after ECAP+CR and ECAP+LTR processing routes. Pure magnesium (Figure 7a) and ZK60+2.5Mm alloy (Figure 7c) processed by ECAP+LTR showed the highest gravimetric capacities after activation with maximal values of hydrogen absorbed fraction of 0.82 and 0.86, respectively.

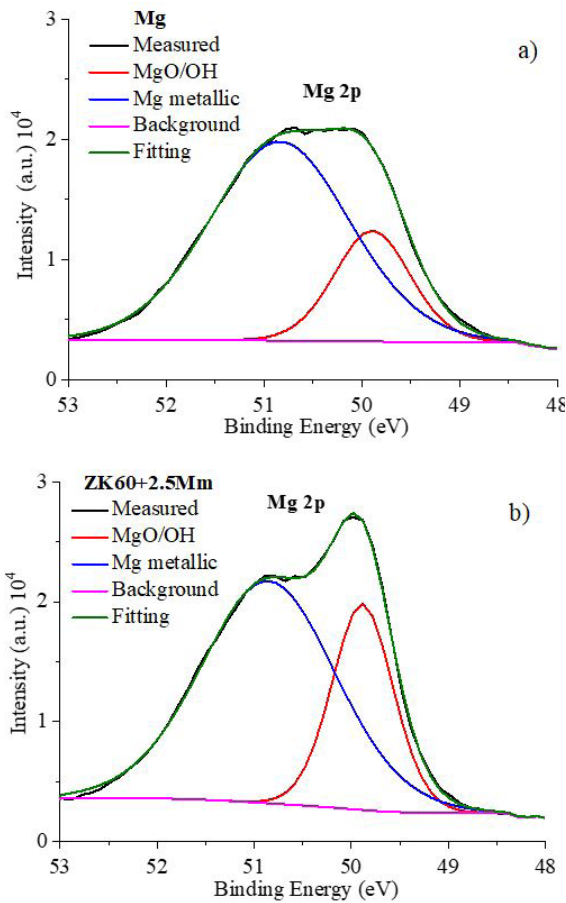


**Figure 6.** XPS spectra of Mg-2p peak for (a) pure Mg and (b) ZK60+2.5 Mm alloy after ECAP+LTR processing routes.

In addition, the ECAP+LTR route showed activation kinetics slightly faster than for ECAP+CR route in both materials. Pure magnesium and ZK60+2.5Mm samples obtained by ECAP+CR could absorb only fractions of 0.65 and 0.50, as shown in Figures 7a, c, respectively. Meanwhile, an incubation period of around 30 min. was observed during activation of the pure Mg, while no incubation time was observed in the ZK60+2.5Mm alloy regardless of the processing route used. This small or no incubation period can be the result of strong crystallographic orientation along to (002) direction, which facilitates the activation in the first stage of hydrogenation<sup>38</sup>. The absence of incubation time for the ZK60+2.5Mm alloy can be associated with the presence of Mm in the alloy that can act as nucleation sites for the hydrogen absorption which possibly inhibits the formation of contaminants species. This reasoning is also in agreement with the XPS analysis (Figure 6) that indicated a slightly larger amount of oxides/hydroxides in pure Mg compared with the alloy.

The first hydrogen desorption kinetics of both magnesium materials was improved by employing the ECAP+LTR route resulting in faster kinetics and more complete desorption. In this case, the pure Mg (Figure 7b) and ZK60+2.5Mm (Figure 7d) samples showed desorbed hydrogen fraction of 0.73 and 0.78 within 1.5 and 1 h, respectively. In addition,

hydrogen was almost entirely desorbed after 30 min in the ZK60+2.5Mm alloy processed by ECAP+LTR. In summary, pure Mg and ZK60+2.5Mm samples processed by the ECAP+CR route exhibited lower hydrogen desorption capacity and slow kinetics when compared with the samples processed by ECAP+LTR. Our results are superior to those reported by Lima et al.<sup>22</sup> that showed a desorption capacity of 4.4 wt% for commercial pure Mg processed by ECAP+CR, which corresponds to 0.58 of the fraction of its theoretical capacity that means a value lower than that verified in this study for ECAP+LTR.

Magnesium has a relatively slow kinetics to react with hydrogen and this may be due to its relatively low ability to either dissociate hydrogen atoms or create a stable surface hydride structure that limits the diffusion of hydrogen atoms into the magnesium matrix<sup>37,38</sup>. As we noticed in the results showed so far, the combined process of ECAP+LTR produced more intense grain refinement than by ECAP+CR, which resulted in larger area of grain boundaries and internal defects (Figure 3, 4, and 5; Table 3) that improved the following hydrogen storage properties such as: absorption capacity and H<sub>2</sub> absorption/desorption kinetics; surface area/volume ratio; increased density of defects; large amount of exposed interfaces. Such improvements caused faster hydrogen diffusion mobility and better desorption-capacity for samples processed by ECAP+LTR than for ECAP+CR. Such results are in good agreement with those obtained by Hongo et al.<sup>51</sup>, who indicated that large crack fractions and grain boundaries can act as pathways to move the hydrogen from the surface into the samples and activate the material with rapid hydrogenation kinetics.

The second cycle of hydrogen absorption/desorption kinetics for pure Mg and for ZK60+2.5Mm alloy after processing by ECAP+CR and ECAP+LR are displayed in Figure 8a, d. Considering only the pure Mg sample, we could see that the sample processed by ECAP+LTR showed higher hydrogen capacity and faster kinetics during the absorption (Figure 8a) and desorption (Figure 8b) compared with the sample processed by ECAP+CR. The worst result was found for the Mg sample processed by ECAP+CR. During desorption, the ECAP+LTR sample reached stability of hydrogen capacity within 1 h.

On the other hand, the ZK60 + 2.5Mm (Figure 8c) alloy exhibited higher hydrogen storage capacity than for pure magnesium. This can be ascribed to the larger grain boundary interface (as can be seen in Figure 4) and, mainly, to the higher relationship between the crack volume fraction ( $V_c$ ) and the reconstructed sample volume ( $V_r$ ) as determined by microtomography reconstructions (seen in Table 3) thus generating a greater surface area/volume ratio of the ZK60+2.5Mm alloy compared with the pure Mg after the ECAP+CR and ECAP+LTR routes. Although the presence of MgO/Mg(OH)<sub>2</sub> contributed to the degradation of the hydrogen storage capacities in the two cycles tested, hydrogen could be absorbed and desorbed easier during the second hydrogenation process. These results indicate that Mm-rich second phase can operate as preferential nucleation centers for hydride development<sup>27, 52</sup>.

After exposure to high (de)hydrogenation temperatures, the number of internal defects in both materials is reduced and

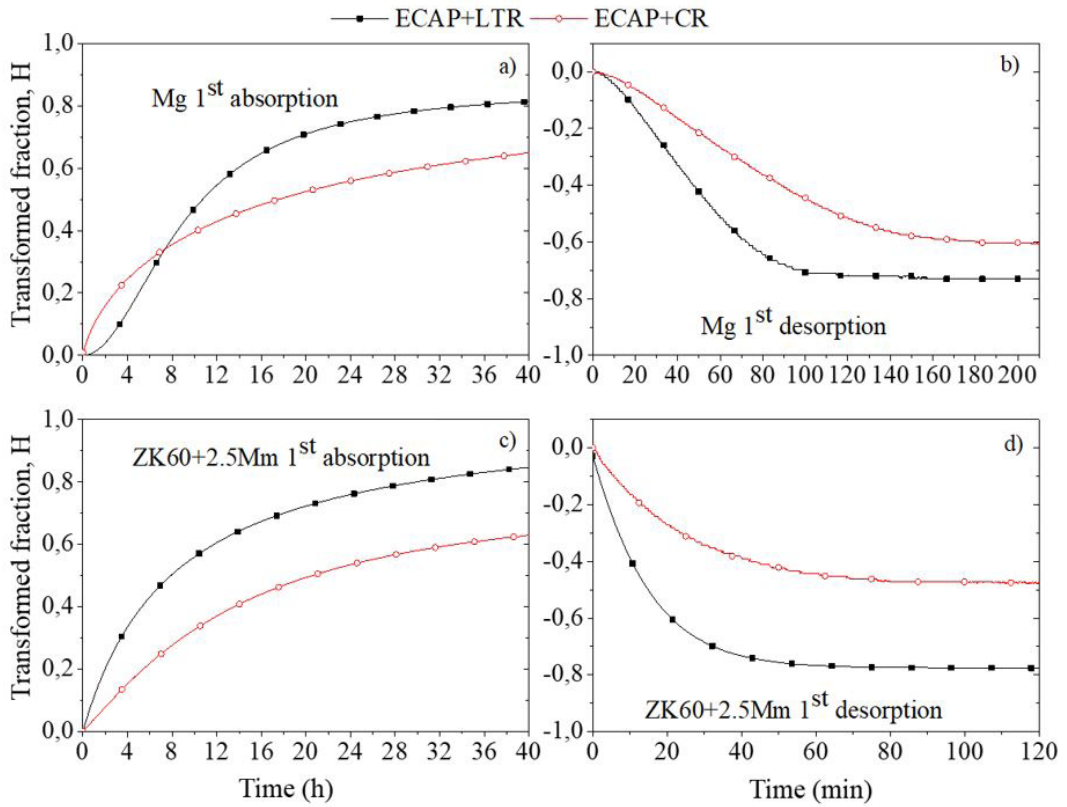


Figure 7. Kinetic curves of (a,c) first absorption (activation) and (b, d) first desorption of pure Mg and ZK60+2.5Mm alloy, respectively.

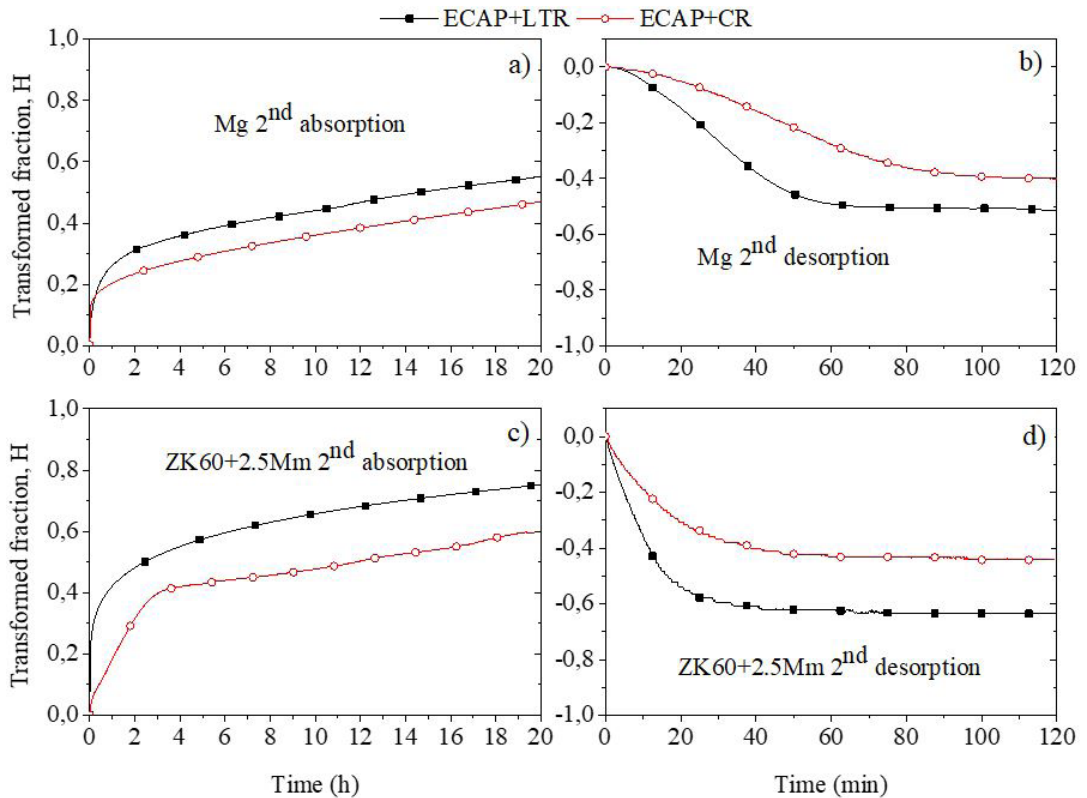


Figure 8. Kinetic curves of (a, c) second absorption and (b, d) second desorption of pure Mg and ZK60+2.5Mm alloy, respectively.

this reduction is expected to be smaller in the ZK60+2.5Mm alloy due to the great incidence of defects and precipitates associated with Zn and Mm, which in certain amount remain stable even at high working temperatures. Grill et al.<sup>53</sup> reported that increasing the distance between nucleation centers and consequently the reduction of them demands longer time for the absorption cycles to reach the full theoretical capacity of the material.

Among the alloys investigated, the ZK60+2.5Mm alloy processed by ECAP+LTR route presented higher hydrogen capacity in comparison with the pure Mg processed by the same route during the activation kinetics.

During second hydrogenation, the ZK60+2.5Mm alloy processed by ECAP+LTR showed higher absorption/desorption hydrogen capacity compared to the pure Mg processed by ECAP+CR and ECAP+LTR. Indeed, the hydrogen storage capacity observed for pure Mg sample decreased from the first to the second cycle in both process routes. One of the reasons for this drop of capacity in Mg pure and Mg-based materials is associated with the hydrogen retained after desorption, which results in less space available for subsequent absorptions - more details can be found in the references<sup>52-53</sup>. In contrast, the ZK60+2.5Mm alloy processed by ECAP+CR and ECAP+LTR maintained its hydrogen capacities from 1<sup>st</sup> to 2<sup>nd</sup> cycle when analyzing 20h of tests.

From these results, we can confirm that the hydrogen storage properties of ZK60+2.5Mm alloy is much better than for the Mg pure especially due to the presence of intermetallic network composed by secondary phases that can act as nucleation sites for the hydride formation. Another interesting point demonstrated in this investigation is regarding to the positive effects on hydrogen storage properties of samples performed by CR+LTR in relation to the CR processing. The CR+LTR processing was very effective to introduce a larger amount of defects such as the dislocation, cracks and new interfaces leading to a more refined microstructure in Mg-based alloys. The processing of ZK60+2.5Mm alloy by CR+LTR resulted in a synergic effect in terms of hydrogen storage properties in comparison with the pure Mg in combination with other processing routes. Not less important, ECAP seems to be a promising preliminary processing route due to its simplicity and also the ability to produce samples with high air-resistance.

## 4. Conclusions

In this study, we evaluate the hydrogen storage properties of pure magnesium and magnesium ZK60 + 2.5 wt.% of mischmetal (Mm) alloys performed by Cold Rolling (CR) and Low Temperature Rolling (LTR). These samples were initially processed by ECAP. The following conclusions could be drawn from this investigation:

- Samples processed through ECAP+LTR showed less ductility than those processed through ECAP+CR, resulting in a larger amount of cracks. Thus, more surfaces and exposed interfaces could be created, especially for the ZK60+2.5Mm alloy as it already has more secondary phase interfaces.
- Processing using both combination routes (ECAP+LTR and ECAP+CR) resulted in  $\alpha$ -Mg grains with a preferred orientation of the (002) basal plane, which

improved the properties for hydrogen storage for both Mg-based materials. However, the planar slip behavior was not the same in both materials, being less intense for ZK60+2.5Mm when compared with pure Mg.

- ZK60+2.5Mm alloy exhibited the best resistance to the formation of oxides (MgO) and hydroxides (Mg(OH)<sub>2</sub>) according to the XPS results. Consequently, there was a larger contaminant-free area, the MgH<sub>2</sub> hydride was formed with faster kinetics, and no incubation time was observed during activation for both materials.
- Compared with CR, LTR induced improvement of the following hydrogen storage properties: absorbed capacity and H<sub>2</sub> absorption/desorption kinetics. The surface area/volume ratio, the increased density of defects, and the larger number of interfaces resulting from the LTR process explain these improvements.
- The processing routes (ECAP + LTR and ECAP + CR) used in this study are not the cheapest for the production of Mg-based materials for hydrogen storage, but they guarantee favorable hydrogen storage conditions for these materials.

## 5. Acknowledgements

The authors acknowledge the Fundação de Amparo à Pesquisa do Estado de S. Paulo-Brazil (FAPESP) (Project No. 2013/05987-8; Regular Project No. 2018/15968-4) and the Coordenação de Aperfeiçoamento de Pessoal de Nível Superior - Brasil (CAPES) - Finance Code 001. This research used resources of the Brazilian Synchrotron Light Laboratory (LNLS), an open national facility operated by the Brazilian Centre for Research in Energy and Materials (CNPEM) a private non-profit organization under the supervision of the Brazilian Ministry for Science, Technology, Innovations and Communications (MCTIC). The IMX Beamline staff and specially Gabriel Schubert is acknowledged for the assistance during the experiments. Authors also thanks the Brazilian Nanotechnology National Laboratory under proposals XPS-21358 and MicroCT-19224 and the Laboratory of Structure and Characterization of the Federal University of São Carlos (LCE/DEMa/UFSCar) for providing access to their facilities.

## 6. References

1. Jain IP, Lal C, Jain A. Hydrogen storage in Mg: a most promising material. *Int J Hydrogen Energy*. 2010;35:5133-44.
2. Zhang F, Zhao P, Niu M, Maddy J. The survey of key technologies in hydrogen energy storage. *Int J Hydrogen Energy*. 2016;41:14535-52.
3. Chanchetti LF, Leiva DR, Lopes de Faria LI, Ishikawa TT. A scientometric review of research in hydrogen storage materials. *Int J Hydrogen Energy*. 2019;45:5356-66.
4. Schlapbach L, Züttel A. Hydrogen-storage materials for mobile applications. *Nature*. 2001;414:353-8.
5. Selvam P, Viswanathan B, Swamy CS, Srinivasan V. Magnesium and magnesium alloy hydrides. *Int J Hydrogen Energy*. 1986;11:169-92.
6. Sakintuna B, Lamari-Darkrim FM, Hirscher M. Metal hydride materials for solid hydrogen storage: a review. *Int J Hydrogen Energy*. 2007;32:1121-40.

7. Klyamkin SN. Metal hydride compositions on the basis of magnesium as materials for hydrogen accumulation. *Russ J Gen Chem.* 2007;77:712-20.
8. Züttel A. Hydrogen storage methods. *Naturwissenschaften.* 2004;91:157-72.
9. Bérubé V, Radtke G, Dresselhaus M, Chen G. Size effects on the hydrogen storage properties of nanostructured metal hydrides: a review. *Int J Energy Res.* 2007;31:637-63.
10. Yao X, Lu G. Magnesium-based materials for hydrogen storage: recent advances and future perspectives. *Chin Sci Bull.* 2008;53:2421-31.
11. Hitam CNC, Aziz MAA, Ruhaimi AH, Taib MR. Magnesium-based alloys for solid-state hydrogen storage applications: a review. *Int J Hydrogen Energy.* 2021;46:31067-83.
12. Leiva DR, Fruchart D, Bacia M, Girard G, Skryabina N, Villela ACS, et al. Mg alloy for hydrogen storage processed by SPD. *Int J Mater Res.* 2009;100:1739-46.
13. Soyama J, Leiva DR, Guo YF, Jorge AM, Da Silva EP, Pinto HC, et al. Severely deformed ZK60 + 2.5% Mm alloy for hydrogen storage produced by two different processing routes. *Int J Hydrogen Energy.* 2016;41:11284-92.
14. Wang L, Jiang J, Ma A, Li Y, Song DA. Critical review of mg-based hydrogen storage materials processed by equal channel angular pressing. *Metals.* 2017;7:324.
15. Asselli AAC, Leiva DR, Huot J, Kawasaki M, Langdon TG, Botta WJ. Effects of equal-channel angular pressing and accumulative roll-bonding on hydrogen storage properties of a commercial ZK60 magnesium alloy. *Int J Hydrogen Energy.* 2015;40:16971-6.
16. Huot J, Skryabina N, Fruchart D. Application of severe plastic deformation techniques to magnesium for enhanced hydrogen sorption properties. *Metals.* 2012;2:329-43.
17. Huot J, Tousignant M. Effect of cold rolling on metal hydrides. *Mater Trans.* 2019;60:1571-6.
18. Silva EP, Leiva DR, Pinto HC, Floriano R, Neves AM, Botta WJ. Effects of friction stir processing on hydrogen storage of ZK60 alloy. *Int J Hydrogen Energy.* 2018;43:11085-91.
19. Leiva DR, Jorge AM, Ishikawa TT, Botta WJ. Hydrogen storage in Mg and Mg-based alloys and composites processed by severe plastic deformation. *Mater Trans.* 2019;60:1561-70.
20. Skripnyuk VM, Rabkin E, Estrin Y, Lapovok R. Improving hydrogen storage properties of magnesium based alloys by equal channel angular pressing. *Int J Hydrogen Energy.* 2009;34:6320-4.
21. Krystian M, Zehetbauer MJ, Kropik H, Mingler B, Krexner G. Hydrogen storage properties of bulk nanostructured ZK60 Mg alloy processed by Equal Channel Angular Pressing. *J Alloys Compd.* 2011;509:S449-55.
22. Leiva DR, Chanchetti LF, Floriano R, Ishikawa TT, Botta WJ. Exploring several different routes to produce Mg-based nanomaterials for Hydrogen storage. *IOP Conf Series Mater Sci Eng.* 2014;63:012115.
23. Lima GF, Triques MRM, Kiminami CS, Botta WJ, Jorge AM. Hydrogen storage properties of pure Mg after the combined processes of ECAP and cold-rolling. *J Alloys Compd.* 2014;586:S405-8.
24. Floriano R, Leiva DR, Melo GC, Ishikawa TT, Huot J, Kaufman JM, et al. Low temperature rolling of AZ91 alloy for hydrogen storage. *Int J Hydrogen Energy.* 2017;42:29394-405.
25. Silva EP, Leiva DR, Floriano R, Oliveira VB, Pinto HC, Botta WJ. Hydrogen storage properties of filings of the ZK60 alloy modified with 2.5 wt% mischmetal. *Int J Hydrogen Energy.* 2020;45:5375-83.
26. Tran NE, Lambrakos SG, Imam MA. Analyses of hydrogen sorption kinetics and thermodynamics of magnesium–misch metal alloys. *J Alloys Compd.* 2006;407:240-8.
27. Poletaev AA, Denys RV, Solberg JK, Tarasov BP, Yartys VA. Microstructural optimization of LaMg12 alloy for hydrogen storage. *J Alloys Compd.* 2011;509:S633-9.
28. Poletaev AA, Denys RV, Maehlen JP, Solberg JK, Tarasov BP, Yartys VA. Nanostructured rapidly solidified LaMg11Ni alloy: Microstructure, crystal structure and hydrogenation properties. *Int J Hydrogen Energy.* 2012;37:3548-57.
29. Darriet B, Pezat M, Hbika A, Hagenmuller P. Application of magnesium rich rare-earth alloys to hydrogen storage. *Int J Hydrogen Energy.* 1980;5:173-8.
30. Yuan JG, Xing N, Wu Y. The effect of Mm content on microstructure and hydrogen storage properties of the as-cast Mg90-xNi10Mmx (x = 1, 2, 3 at.%) alloys. *Int J Hydrogen Energy.* 2017;42:6118-26.
31. Silva EP, Marques F, Nossa TS, Alfaro U, Pinto HC. Impact of Ce-base mischmetal on the microstructure and mechanical behavior of ZK60 magnesium casting alloys. *Mater Sci Eng A.* 2018;723:306-13.
32. Langdon TG, Furukawa M, Nemoto M, Horita Z. Using equal-channel angular pressing for refining grain size. *JOM.* 2000;52:30-3.
33. Miqueles E, Koshev N, Helou ES. A backprojection slice theorem for tomographic reconstruction. *IEEE Trans Image Process.* 2017;27:894-906.
34. Asselli AAC, Hébert NB, Huot J. The role of morphology and severe plastic deformation on the hydrogen storage properties of magnesium. *Int J Hydrogen Energy.* 2014;39:12778-83.
35. Silva EP, Buzolin RH, Callegari B, Warchomicka F, Requena GC, Pinto HC. Effect of mischmetal additions and solution heat treatments (T4) on the microstructure and mechanical properties of thixocast ZK60 - RE magnesium alloys. *Trans Tech Publ.* 2016;879:2300-5.
36. Silva EP, Batista LF, Callegari B, Feierabend I, Buzolin RH, Coelho RS, et al. Casting in the semi-solid state of ZK60 magnesium alloy modified with rare earth addition. *Adv Mat Res.* 2014;922:694-9.
37. Jiang Y, Chen D, Chen Z, Liu J. Effect of cryogenic treatment on the microstructure and mechanical properties of AZ31 magnesium alloy. *Mater Manuf Process.* 2010;25:837-41.
38. Léon A, Knystautas EJ, Huot J, Schulz R. Influence of the evaporation rate and the evaporation mode on the hydrogen sorption kinetics of air-exposed magnesium films. *Thin Solid Films.* 2006;496:683-7.
39. Jorge AM, Lima GF, Triques MRM, Botta WJ, Kiminami CS, Nogueira RP, et al. Correlation between hydrogen storage properties and textures induced in magnesium through ECAP and cold rolling. *Int J Hydrogen Energy.* 2014;39:3810-21.
40. Jorge AM, Prokofiev E, Lima GF, Rauch E, Veron M, Botta WJ, et al. An investigation of hydrogen storage in a magnesium-based alloy processed by equal-channel angular pressing. *Int J Hydrogen Energy.* 2013;38:8306-12.
41. Soyama J, Triques MRM, Leiva DR, Jorge AM, Da Silva EP, Pinto HC, et al. Hydrogen storage in heavily deformed ZK60 alloy modified with 2.5 wt.% Mm addition. *Int J Hydrogen Energy.* 2016;41:4177-84.
42. Huot J, Amira S, Lang SJ, Skryabina N, Fruchart D. Improvement of hydrogen storage properties of magnesium alloys by cold rolling and forging. *IOP Conf Series Mater Sci Eng.* 2014;63:012114.
43. Lang J, Skryabina N, Fruchart D, Danaie M, Huot J. Microstructure of cold rolled Magnesium and Magnesium hydrides for hydrogen storage applications. *Chemistry for Sustainable Development.* 2013;21:1-8.
44. Figueiredo RB, Langdon TG. Grain refinement and mechanical behavior of a magnesium alloy processed by ECAP. *J Mater Sci.* 2010;45:4827-36.
45. Edalati K, Cubero-sesin JM, Alhamidi A, Mohamed IF, Horita Z. Influence of severe plastic deformation at cryogenic temperature on grain refinement and softening of pure metals: investigation using high-pressure torsion. *Mater Sci Eng A.* 2014;613:103-10.
46. Danaie M, Mauer C, Mitlin D, Huot J. Hydrogen storage in bulk Mg–Ti and Mg–stainless steel multilayer composites synthesized

- via accumulative roll-bonding (ARB). *Int J Hydrogen Energy*. 2011;36:3022-36.
47. Maeda MY, Quintero JJH, Izumi MT, Hupalo MF, Cintho OM. Study of cryogenic rolling of FCC metals with different stacking fault energies. *Mater Res*. 2017;20:716-21.
  48. Zhiquan H, Jianchun W, Qingxue H, Lifeng M, Xiangyu G, Zhaohan Y. Effect of cryogenic treatment prior to rolling on microstructure and mechanical properties of AZ31 magnesium alloy. *Rare Met Mater Eng*. 2018;47:2942-8.
  49. Friedrichs O, Sánchez-LópezB JC, López-Cartes C, Dornheim MT, Klassen T, Bormann R, et al. Chemical and microstructural study of the oxygen passivation behaviour of nanocrystalline Mg and MgH<sub>2</sub>. *Appl Surf Sci*. 2006;252:2334-45.
  50. Vincent SD, Huot J. Effect of air contamination on ball milling and cold rolling of magnesium hydride. *J Alloys Compd*. 2011;509:L175-9.
  51. Hongo T, Edalati K, Arita M, Matsuda J, Akiba E, Horita Z. Significance of grain boundaries and stacking faults on hydrogen storage properties of MgNi intermetallics processed by high-pressure torsion. *Acta Mater*. 2015;92:46-54.
  52. Sadhasivam T, Hudson MSL, Pandey SK, Bhatnagar A, Singh MK, Gurunathan K, et al. Effects of nano size mischmetal and its oxide on improving the hydrogen sorption behaviour of MgH<sub>2</sub>. *Int J Hydrogen Energy*. 2013;38:7353-62.
  53. Grill A, Horky J, Panigrahi A, Krexner G, Zehetbauer M. Long-term hydrogen storage in Mg and ZK60 after Severe Plastic Deformation. *Int J Hydrogen Energy*. 2015;40:17144-52.